A film-forming graphene/diketopyrrolopyrrole covalent hybrid with far-red optical features: Evidence of photo-stability

A film-forming graphene/diketopyrrolopyrrole covalent hybrid with far-red optical features: evidence of photo-stability

Meng Zheng [a], Francesco Lamberti [b,c], Lorenzo Franco [a], Elisabetta Collini [a], Ilaria Fortunati [a], Gregorio Bottaro [a,d], Giorgia Daniel [a], Roberto Sorrentino [e], Alessandro Minotto [f], Akos Kukovecz [g], Enzo Menna [a,c], Simone Silvestrini [a], Christian Durante [a], Franco Cacialli [f], Gaudenzio Meneghesso [b,c], Michele Maggini [a], Teresa Gatti [h]*

[a] Department of Chemical Sciences, University of Padova and INSTM UdR Padova, via Marzolo 1, 35131 Padova, Italy

[b] Department of Information Engineering, University of Padova, Via Gradenigo 6/B, 35131 Padova, Italy

[c] Interdepartmental Centre Giorgio Levi Cases for Energy Economics and Technology, Via Marzolo 9, 35131 Padova

[d] CNR ICMATE, Department of Chemical Sciences, University of Padova and INSTM UdR Padova, via Marzolo 1, 35131 Padova, Italy

[e] Istituto per lo Studio delle Macromolecole (ISMac-CNR), Via Bassini 15, 20133, Milano, Italy

[f] Department of Physics and Astronomy and London Center for Nanotechnology, University College London, London, WC1E 6BT, United Kingdom

[g] University of Szeged, Interdisciplinary Excellence Centre, Department of Applied and Environmental Chemistry, H-6720, Rerrich Béla tér 1, Szeged, Hungary

[h] Institute of Physical Chemistry and Center for Materials Research, Justus Liebig University Giessen, Heinrich-Buff-Ring 17, 35392 Giessen, Germany

E-mail: teresa.gatti@phys.chemie.uni-giessen.de

Abstract

A dianiline derivative of a symmetric donor-acceptor-donor diketopyrrolopyrrole-based dye is employed for the two-sided covalent functionalization of liquid exfoliated few layers graphene flakes, through a direct arylation reaction. The resulting nanohybrid features the properties of a polymeric species, being solution-processed into homogeneous thin films, featuring a pronounced red-shift of the main absorption band with respect to the model dye unit and energy levels comparable to those of common diketopyrrolopyrrole-based polymers. A good electrical conductivity and the absence of radical signals generated after intense white light illumination, as probed through electron

paramagnetic resonance, suggest a possible future application of this composite material in the field of photoprotective, antistatic layers with tunable colors.

Keywords

Functional nanocarbon hybrids, liquid exfoliated graphene, diketopyrrolopyrrole, nanocomposites, hybrid nanomaterials

1. Introduction

The hybridization of graphene-based materials (GBM) with organic semiconductors (OSC) is at the center of multiple research efforts worldwide, with the aim of defining novel platforms for optoelectronic architectures that can combine the robustness and high conductivity of the former with the tunable optical properties of the latter.[1] Interesting examples include the coupling with photochromic molecules,[2][3] to modulate conductivity and charge-transfer processes through selective illumination,[4] the blending with donor-acceptor mixtures in organic photovoltaic devices, to tune the electron-cascade process after photoexcitation[5] and the mixing with polymeric hole-transporting species to improve charge extraction and stability in perovskite solar cells.[6,7] Some of us have also reported the use of a covalent functional nanocarbon hybrid[8] based on reduced graphene oxide (RGO) and an organic donor-π-acceptor chromophore as photosensitizers in classical dye sensitized solar cells (DSSC),[9] achieving efficient photoinduced electron-transfer into a high-band metal oxide semiconductor acceptor,[10] a discrete photocurrent and good perspectives for solar cell stability. This last one was suggested by the remarkable resistance of the RGO-containing species to highly aggressive liquid environments, such as those existing in liquid electrolyte-based DSSC. In addition, the covalent anchoring of the chromophore to the GBM scaffold further ensures robustness to the hybrid structure.

The opportunities offered by covalent chemistry for the construction of GBM-OSC hybrids and composites are indeed multiple, given the large number of chemical reactions that can be exploited, as well as the type and topology of reactive centers on the GBM that can be involved.[11–13] Whereas reactions at oxygenated defect-sites are generally of the condensation-type (esterifications, amidations), C-C double bonds can also be targeted as reactive centers within a bulk GBM structure. In this context, it is particularly interesting for the fast kinetic[14] and the possibility of *in-situ* realization, the direct arylation reaction (also called Tour-reaction,[15] initially developed on carbon nanotubes but applicable also to GBM substrates). This reaction makes use of an aniline derivative as the functionalizing agent, in combination with isoamyl nitrite, to directly produce in the reaction mixture the diazonium salt, which in this way does not need to be isolated. It then exploits the electron

donating ability of the sp^2 carbon-based substrate to *in situ* reduce the diazonium salt, eliminate molecular nitrogen and generate an aryl radical, able to react with C-C double bonds and generate sp^3 carbon sites. This reaction was employed in many different contexts, provided that a source of electrons is present:[16] for example, some of us have recently enriched its versatility by applying it in microfluidic reactors for the covalent functionalization of RGO with organic dyes.[17] This approach is undoubtedly promising for scaling-up the production of GBM-OSC hybrids, allowing a tight control on temperature, reaction times and reactant quantities, which are key factors for tuning the morphology of the functionalization.

In this work, we make use of a bi-functional OSC molecule to produce with few layers graphene flakes a covalent nanohybrid that shows some clear features of a polymeric material. We define the process as a cross-linking, in that the bi-functional OSC molecule can bind from two opposites sides to graphene surfaces.[18,19] Such an OSC is indeed a symmetric dianiline derivative of a bithiophene-diketopyrrolopyrrole molecule (see Figure 2), a donor-acceptor-donor (D-A-D) system, characterized by optimal light-absorption in the visible range, strong fluorescence and good solubility in a large plethora of organic solvents. Diketopyrrolopyrrole A units, as parts of both single-molecule and polymer scaffolds, have been largely investigated for several optoelectronic applications, such as organic photovoltaics,[20–22] organic thin film transistors,[23] organic light emitting diodes [24,25] and fluorescent sensors.[26] They are nowadays some of the most studied OSC because of their synthetic versatility, that allows the tuning of both intra and intermolecular properties by, respectively, modifying the D units to which they are bound in the 2-positions and the functional groups that decorate the two nitrogen atoms. In particular, while the change in D units can allow the tuning of the band-gap,[27] the modification of the groups attached to nitrogen can either induce the formation of hydrogen bonds (when such a group is hydrogen) with carbonyl groups on sister molecules,[28,29] or tune the type of aggregates that are formed in the solid state (when linear/branched alkyl chains or other groups are introduced).[30,31]

The graphene/diketopyrrolopyrrole hybrid that we present here appears suitable for paving the way to a new class of organic composite materials that could find application as anti-static, photo-protective coatings,[32] in that it presents a good conductivity,[33] associated with broad absorption features across the UV-visible-NIR range and good photo-stability to intense irradiation. In addition, the film-forming ability, the semi-transparency of the resulting films and the possibility to tune the color by changing the OSC used for cross-linking,[34] are other peculiarities of this new generation of carbon-based materials, which might be commercialized in the future as a particular class of organic anti-static coatings.[35]

2. Experimental Section

2.1 Materials and Methods

All commercially available reagents and solvents were purchased from Sigma–Aldrich, Fluka and TCI Chemicals and used as received. Graphene powder was purchased from Superior Graphite and used as received. The experimental details on the synthesis of the different thiophene-diketopyrrolopyrrole molecules described in this work are given in the Supporting Information (S.I.). 4-[(3-octyloxy]aniline was synthesized according to a previously reported procedure.[6] Mechanical exfoliation was performed with an IKA T25 Digital Ultra-Turrax® apparatus equipped with an S 25 N – 25 F dispersing tool with a stator diameter of 25 mm. Ultracentrifugation is performed on an MR23i Jouan ultracentrifuge equipped with an SWM 180.5 swinging bucket rotor (Thermo Electron Corporation). NMR spectra were recorded using a Bruker AV III 500 spectrometer operating at 500 MHz for 1H and 125 MHz for 13C (301 K) and a Bruker Avance 300 spectrometer operating at 300 MHz for 1H, 75 MHz for 13C (301K). ESI-MS mass spectra were obtained with Agilent Technologies 1100 Series system equipped with a binary pump (G1312A) and MSD SL Trap mass spectrometer (G2445D SL). The eluents used were MeOH or ACN, both with 0.5% formic acid. UV-visible-NIR spectra were recorded on Varian Cary 5000 spectrophotometer. Steady-state photoluminescence (SS-PL) spectra in solution were recorded on a Horiba Scientific Fluorolog 3 spectrofluorometer equipped with a double grating excitation spectrometer and an iHR320 imaging spectrometer (600 l/mm grating, blaze 1000 nm) coupled to an Horiba Syncerity CCD detector. A 450W Xe arc-lamp was used as excitation source. The emission spectra were corrected for detection and optical spectral response of the spectrofluorimeter supplied by the instrument manufacturer. Time-resolved photoluminescence (TR-PL) measurements in solution were carried out by exciting samples at 400 nm, using a frequency-doubled Ti:Sapphire laser (Coherent, Mira-900S, 76MHz). The emission, filtered by a 600 nm longpass filter, was sent to an avalanche photodiode, connected to a fast electronic for Time-correlated single photon analysis (PicoQuant, PicoHarp 300). Lifetime decays were analyzed with the Symphotime software (PicoQuant) using a two-component fitting model. Fluorescence lifetime imaging microscopy (FLIM) was carried out on a confocal laser scanning microscope (Olympus FV300-IX71) coupled to the same TCSPC electronics by PicoQuant. The excitation laser beam was focused on the film samples through a water immersion 60X microscope objective. The FLIM analysis was performed using a pixel-by-pixel two-exponential reconvolution fit procedure. The presence of SS-PL signal in the near-infrared range (900-1700 nm) was checked with an Ocean Optics NIRQuest 512 spectrometer by exciting the samples at 445 and 520 nm with Thorlabs laser diodes (Power < 5 mW). Micro-Raman spectra were collected with an Invia Renishaw Raman micro spectrometer (X50 objective) using the 633 nm line of a He – Ne laser. A drop of material suspended or dissolved in a given solvent was deposited on a silicon wafer and

placed at the flat bottom of a specifically fabricated flask, which was connected to the vacuum line for solvent evaporation, leaving the cast solid for Raman analysis. Thermogravimetric analysis (TGA) was run on ~1 mg sample using a Q5000 IR model TA instrument with the method of starting at 100 °C and kept isothermal for 20 min, then ramping to 10 °C min^{-1} up to 1000 °C. Dynamic light scattering (DLS) analysis was carried out on a Zetasizer Nano S (Malvern Instruments) operating at 20 °C. Low resolution transmission electron microscopy (TEM) images were recorded on a FEI Tecnai G2 microscope operating at 100 kV. High resolution TEM was performed on a FEI Tecnai G2 20 X Twin instrument operated at a 200 kV accelerating voltage. Samples were drop-cast onto copper mounted holey carbon standard TEM grids. Several different positions were examined on each sample and images were taken at each position. Data presented here represent the most characteristic examples of these measurements. Scanning electron microscopy (SEM) characterization on spin-coated thin films on indium tin oxide (ITO) was carried on an ultra-high vacuum Zeiss Supra 40 with GEMINI column FE-SEM. An electron energy of 3–5 kV, a distance from the sample around 4 mm and a magnification between 20 and 200 k were employed. A high efficiency In-Lens secondary electron detector was used during the images acquisition. The thickness of spin cast layers was measured using KLA-Tencor Alpha-Step IQ Surface Profiler on glass. The scanned lengths were 500 µm with a speed of 40 µm s^{-1} and a rate of sampling of 50 Hz. The reported value is the average of four measurements done in different points of the same sample.

2.2 Mechanical exfoliation of graphite in liquid

Madagascar graphite powder (5 g) was introduced into a 150 mL quartz cylinder with 100 mL N-cyclohexyl-2-pyrrolidone (CHP). The quartz cylinder was arranged in an ice bath to avoid rapid heat release during operation. The high-speed homogenizer was set at a speed of 3000 rpm that was gradually increased to 8000 rpm. After shearing for 20 minutes at 8000 rpm, the suspended material was collected in a centrifuge tube and the dark suspension was centrifuged at 800 rpm (83 x g) for 2 hours. The mixture was then left in the tube overnight to allow sedimentation. The upper suspension was separated from the precipitate and transferred to another tube, while the precipitate was discarded (step 1). The upper suspension collected in step 1 was further centrifuged at 1500 rpm (293 x g). After 2 hours centrifugation, the precipitate was separated from the supernatant and re-suspended in 20 mL of CHP (step 2). This last suspension was marked as EXG 800 and characterized. The supernatant obtained after removing the precipitate in step 2 was further centrifuged at 3000 rpm (1170 x g) for 2 hours (step 3). The precipitate was separated from the supernatant and re-suspended again in 20 mL CHP. This subsequent suspension was marked as EXG 1500 and use for characterization. The supernatant after removing precipitate in step 3 was marked as EXG 3000 and characterized. The concentration of EXG 3000 in CHP was determined by weighting with the thermogravimetric

analyzer the solid residue of 1 mL ink after evaporating the solvent in vacuum. The operation was repeated 3 times, allowing to extract an average value of the concentration equal to 290 ± 8 μg ml^{-1}.

2.3 Synthesis of graphene-diketopyrrolopyrrole covalent hybrids

The EXG 3000 ink (34 ml, ~10 mg of graphene, ~0.84 mmol of C) was transferred to a 250 ml double-necked round-bottom flask kept under nitrogen. 260 mg (0.42 mmol) of the dianiline derivative of bithiophene-diketopyrrolopyrrole (or 300 mg, 0.42 mmol of the monoaniline derivative) and 23 mg of 4-[(2-ethyl)hexyloxy]aniline (0.42 mmol) were then added to the ink and the mixture was stirred and heated up to 80 °C. After reaching the desired temperature, isoamyl nitrite (55 μL, 0.42 mmol) was further added and the reaction was continued for 4 h. After cooling down to room temperature, the mixture was treated with methanol (200 mL) and stirred for 15 min. The covalent hybrid was recovered by filtration on Fluorophore TM membrane filters (0.2 mm, Merck Millipore) and washed with methanol (200 ml). The solid was dried with an IR lamp on the filter and subjected to Soxhlet extraction for further purification with methanol (100 ml), acetone (100 ml) and diethylether (100 ml). Washing and extractions with DMF, chlorinated solvents and toluene were avoided, due to pronounced solubility of the material in this media.

2.4 Electrical characterization

Electrical measurements were conducted on spin cast thin films prepared in a nitrogen-filled glove box. 60 μL of 5 mg ml^{-1} solutions were spun with a speed of 2000 rpm for 30 seconds on a substrate previously exposed for 5 min to an O_2 plasma. The substrates are made of corning glass with interdigitated gold electrodes homemade by photolithography, with channel lengths of 5 μm and width of 20 mm. The electrical measurements were also performed in glove box. By using an Agilent B1500 Semiconductor Parameter Analyzer, a scan voltage from 0 to 3V was applied and the current measured.

2.5 Electron paramagnetic resonance characterization

Samples for electron paramagnetic resonance (EPR) were prepared by inserting toluene solutions (1 mg ml^{-1}) of the materials in quartz tubes (for EXG 3000 the native ink in CHP was directly used), degassing with nitrogen and sealing, to avoid the presence of oxygen. EPR spectra were recorded using a Bruker ER200D spectrometer, operating at x-band (~9.4 GHz), equipped with a nitrogen flow sample temperature controller. All spectra reported have been recorded at T=130K temperature, to improve the signal to noise ratio. Similar results, although much less intense, were obtained at room temperature. Typical spectrometer settings were: sweep 200 Gauss, microwave power 2 mW, field modulation amplitude 2 Gauss, 25 scans. Light Excitation for light-induced EPR spectra has been obtained using white light from a Xenon lamp (LOT Oriel, 300W), IR filtered and focused into an optical fiber delivering about 50 mW of light power to the samples in the EPR spectrometer cavity.

The light-induced EPR spectra are obtained as the difference between the spectra under illumination of the sample ("light ON" spectrum) and the spectrum obtained before illumination of the sample ("dark" spectrum).

3. Results and discussion

Few layers graphene flakes were obtained by applying a mechanical exfoliation protocol in liquid,[36] starting from commercially available Madagascar graphite. This method allows obtaining GBM with a limited number of defects,[37] differently from chemical methods that produce species such as RGO, characterized by holes and wrinkles in the basal plane of the flakes, as a consequence of the oxidation/reduction processes carried out on pristine graphite.[38] In Figure 1a a schematic representation of the exfoliation process is reported, that employs an apparatus for shear mixing in N-cyclohexylpyrrolidone (CHP) liquid medium, which was previously found to be the best solvent for this process.[36] Given the heterogeneous nature of the exfoliation products present in suspension after this initial step, three subsequent centrifugation steps are applied, at progressively higher speed, to isolate a final fraction made of flakes with the smallest number of graphene layers. Characterization of the three fraction of exfoliated graphene (EXG), named after the centrifugation speed used for isolating each of them (and thus, respectively, EXG 800, EXG 1500 and EXG 3000), was carried out through analysis of the 2D band of Raman spectra, for determining the number of layers as reported by Ferrari and coworkers,[39] through TEM for gaining a qualitative information on flakes lateral sizes and through TGA for inferring thermal stability. Figure 1b and 1c report the electron microscopy images of the pristine graphite employed and of the most exfoliated fraction (EXG 3000). As it can be easily recognized (Figure 1c top), by starting from big graphite pieces, large graphene flakes are obtained with this technique, with lateral sizes up to 50 µm or even more, indicating that the process is not disrupting much of the original structure, but simply exfoliating. In the high resolution TEM images (Figure 1c bottom), edges of the flakes are evidenced, from which it is possible to recognize the presence of some graphene mono-layers.

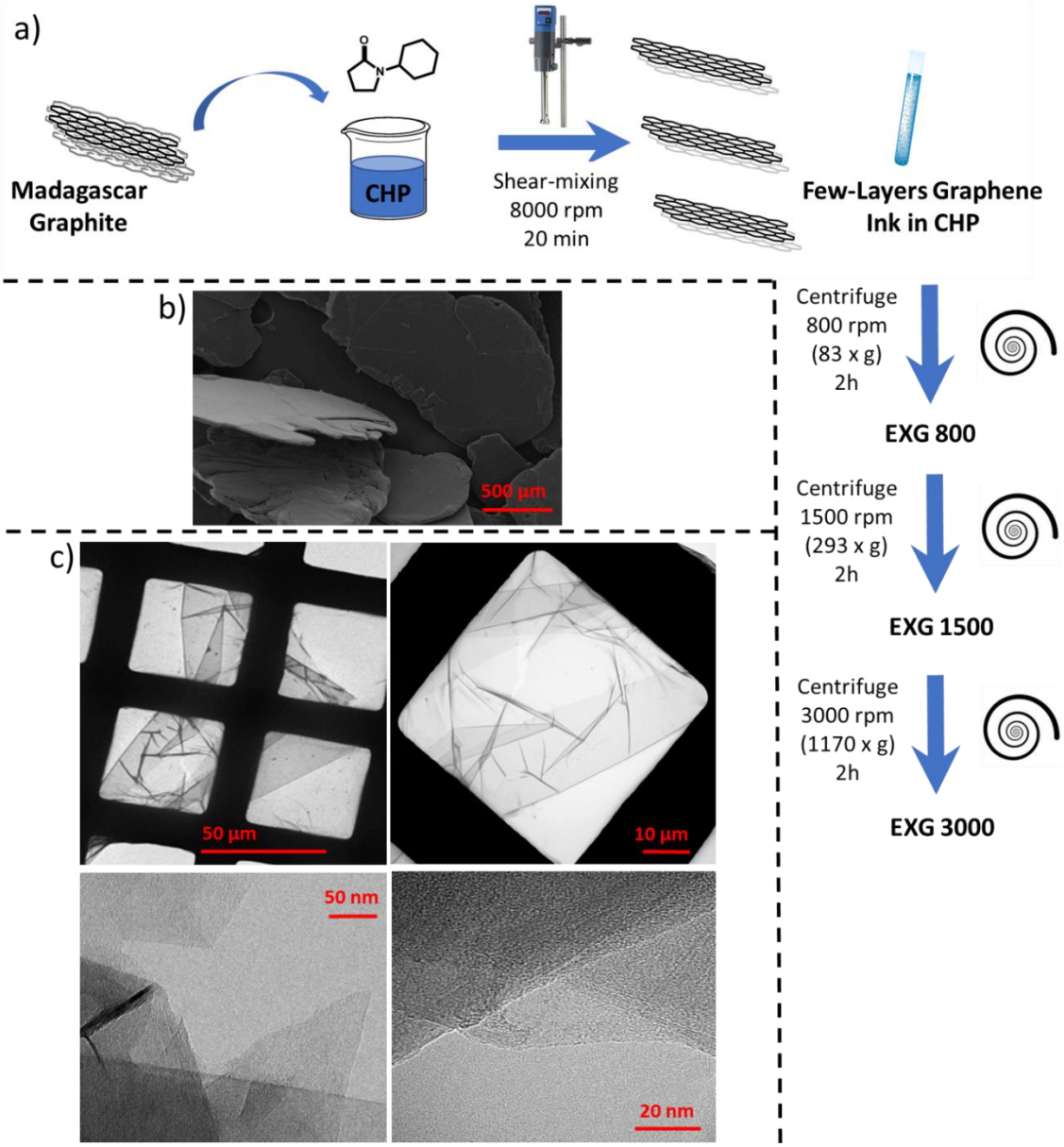

Figure 1. a) Sketch of the graphite mechanical exfoliation procedure employed in this work for the production of a few layers graphene flakes. b) SEM image of the pristine Madagascar graphite. c) Low-resolution (top two) and high-resolution (bottom two) TEM images of the most exfoliated fraction (EXG 3000).

The analysis of the 2D Raman peak (Figure S1a in the S.I. The discussion on D and G band in EXG 3000 is reported later in the text), indicates for the EXG 3000 fraction an average number of graphene layers between 2 and 5, following Ferrari's analysis.[39] For comparison, in the same figure is also reported the 2D Raman signal of the pristine graphite and of a reference single layer graphene sample obtained from chemical vapor deposition (CVD SLG). The EXG 800 and 1500 fractions, intermediate between graphite and EXG 3000, have very similar 2D Raman signatures of 5 to 10 layers species. The thermograms of the three collected fractions are reported in Figure S1b. Also from this analysis a trend emerges, that shows how decomposition temperatures, taken at the onset of decomposition

(see Figure S1b) , decrease progressively with the decrease in the number of layers, with the EXG 3000 fraction having the lowest value at around 590 °C.

The synthesis of the graphene/diketopyrrolopyrrole hybrid, employing the most exfoliated fraction obtained after graphite shear mixing (EXG 3000) and the dianiline derivative of bithiophene-diketopyrrolopyrrole (TDPP) is schematized in Figure 2. The TDPP species employed is a rare example of diketopyrrolopyrrole-based materials bearing secondary alkyl chains bound to the nitrogen atoms. A co-functionalization with simple units of 4-(3-octyloxy)aniline, having analogous alkyl chain to those present on the TDPP moieties, was envisaged to improve solubility of the resulting composite products. The process of *in-situ* direct arylation is interpreted in the present case as a chemical cross-linking of graphene flakes by means of the bifunctional OSC species and the simplified structure of the product is depicted in blue in Figure 2, named *c*-EXG-TDPP (with *c*-indicating the cross-linking). For sake of comparison, a similar species was synthesized, employing a monoaniline derivative of TDPP, able to graft to the graphene surface from one single side. This species is named EXG-TDPP and depicted in purple in Figure 2. For these two graphene/TDPP hybrids, also two corresponding model TDPP small molecules were synthesized, with two and one phenyl group, respectively (Ph_2TDPP in magenta and PhTDPP in pink, Figure 2).

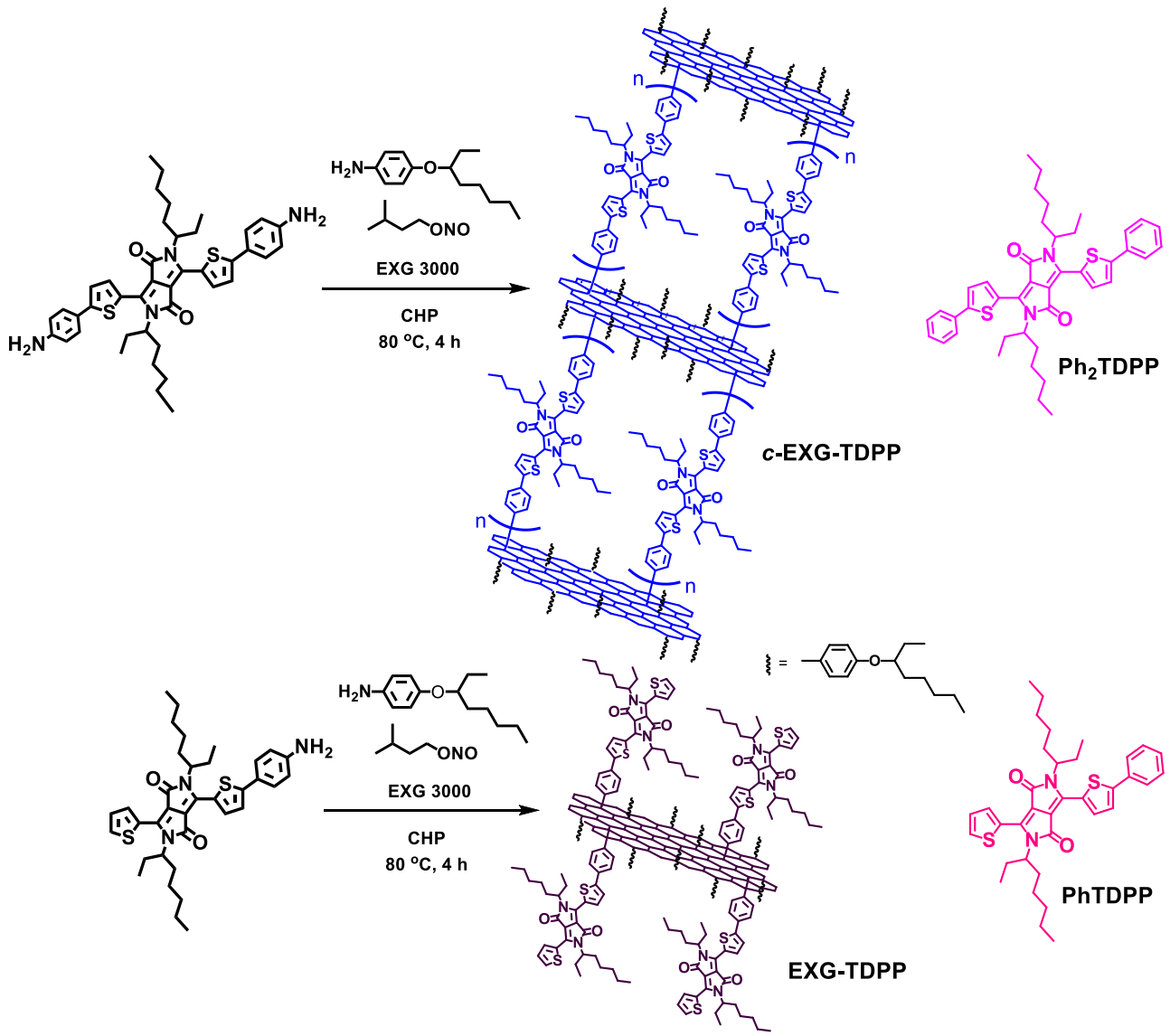

Figure 2. Synthesis of the cross-linked graphene-diketopyrrolopyrrole hybrid (*c*-EXG-TDPP, blue) and of the reference material lacking cross-linking (EXG-TDPP, purple). Both the graphene-diketopyrrolopyrrole hybrids are obtained through *in-situ* direct arylation starting from EXG 3000 and the corresponding di- and monoaniline derivatives. The materials are co-functionalized with 4-[(2-ethyl)hexyloxy]phenyl moieties to improve the solubility. The structure of the two corresponding reference small molecules, Ph_2TDPP and PhTDPP, is also reported for the sake of clarity.

The light-absorption properties of the synthesized hybrids are evaluated in comparison to the model dyes and pristine EXG 3000. Figure 3a reports the absorption spectra of all these species in DMF solution, while Figure 3b shows the visual appearance of these solutions (EXG 3000 not shown, being completely black).

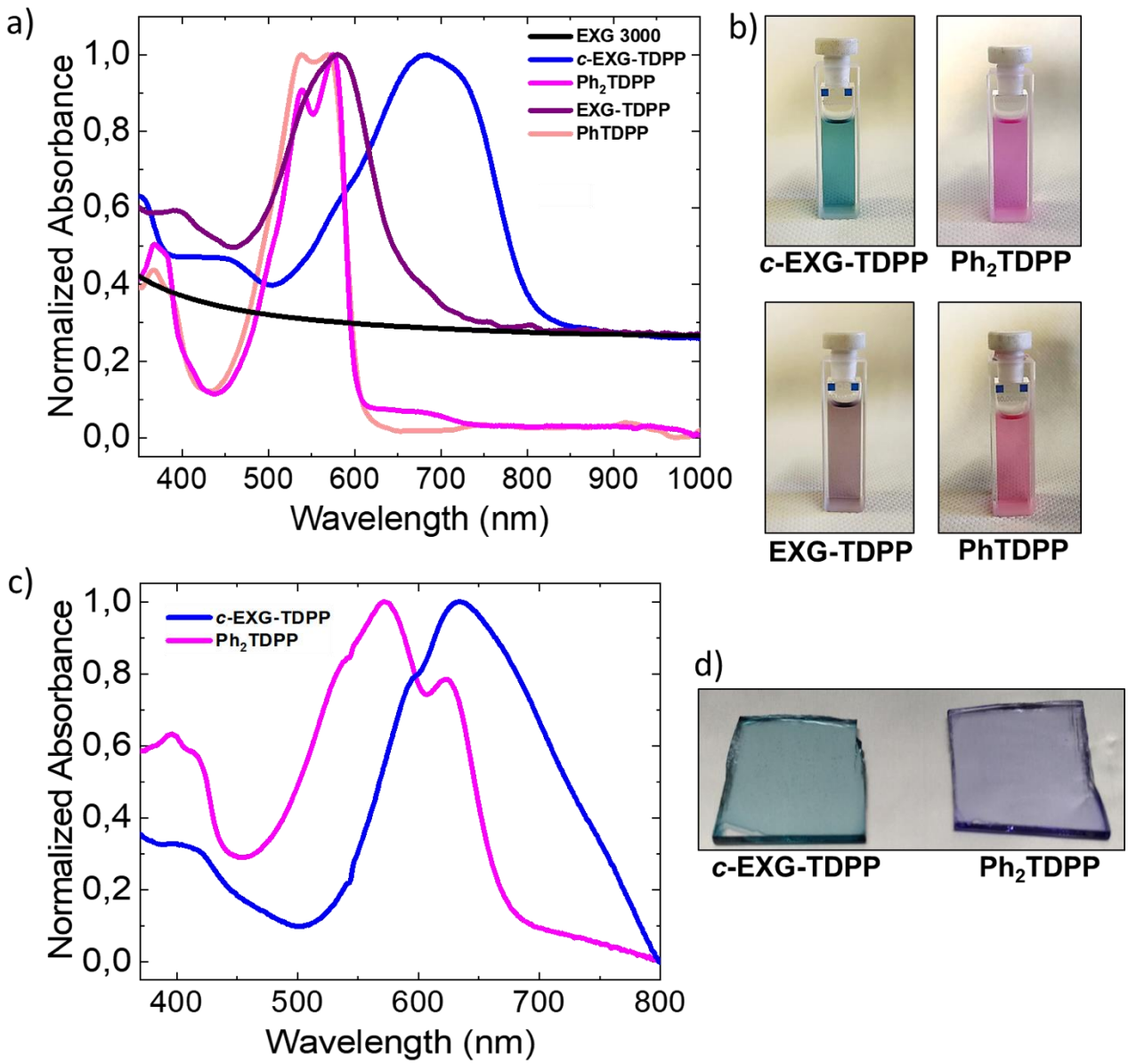

Figure 3. Optical characterization of the graphene-diketopyrrolopyrrole hybrids compared to reference small molecules and pristine EXG 3000. a) Normalized UV-Vis-NIR absorption spectra of the hybrids and of the corresponding reference small molecules in DMF solutions. The spectrum of EXG 3000 is also reported for comparison (a drop of the ink in CHP was diluted with DMF to record the spectrum). b) Photos showing the appearance of the DMF solutions of the graphene-diketopyrrolopyrrole hybrids and of their reference small molecules. c) Normalized UV-Vis absorption spectra of the cross-linked graphene-diketopyrrolopyrrole hybrid and of its reference small molecules in spin-coated thin films obtained from toluene solutions on glass slides. The pictures of these films are reported in d).

These spectra clearly pinpoint the strong red-shift of the main absorption band characteristic of the cross-linked derivative *c*-EXG-TDPP compared to all the other OSC-based species. This band is due to the presence of the covalently attached dye moieties and it is superimposed on a continuous absorption from UV to NIR due to the graphene-based scaffold. Numerically, this shift, taken at the absorption maxima, results to be 108 nm with respect to the reference Ph_2TDPP small molecule (λ_{max}

= 683 vs 575 nm, respectively). While a shift is commonly expected for chromophores covalently bound to GBM,[9,10,17] the one find here is dramatically pronounced. This is further evident if the case of the not cross-linked hybrid is considered. Indeed, for EXG-TDPP compared to its reference PhTDPP chromophore, a shift of the main absorption band of only 12 nm is found (λ_{max} = 581 vs 569 nm). The large red shift in *c*-EXG-TDPP is most likely due to the presence of a polymeric species in solution, as such a value for absorption maxima is also found in TDPP-based conjugated polymers.[40,41] By examining electrochemical data obtained from cyclic voltammetry (see Table S1 for the extrapolated data and Figure S2 for the experimental voltammograms in the S.I., where also a description of the employed procedures is reported), the range of HOMO/LUMO values for *c*-EXG-TDPP (-5.4/-4.1 eV) is in agreement with those of TDPP-based polymers,[40,41] but a smaller HOMO-LUMO electrochemical gap is found for the hybrid with graphene (1.27 eV vs ~ 2 eV). This points out at the existence of some additional effects on the overall conjugation of the system deriving from the presence of the graphene component.

The polymeric nature of the cross-linked hybrid further emerges when the high solubility in many different organic solvents (toluene, chlorobenzene, chloroform, dichloromethane, DMF) and the excellent film-forming ability is considered. Figure 3b shows the typical appearance of a spin-cast film of *c*-EXG-TDPP, together with that of the reference small molecule Ph_2TDPP, whose thicknesses were evaluated to be 150 ±30 nm and 120 ±20 nm, respectively. For comparison, attempts to obtain homogeneous thin films of the not cross-linked derivative failed. Indeed, this species has the tendency to produce big aggregates (visible to the naked eye) and it is unlikely a polymer or a polymer composite. Figure 3c shows the absorption spectrum of a *c*-EXG-TDPP film, which presents many similarities with the corresponding spectrum in solution, with no clear evidence of continuous graphene absorption. The spectrum of the spin-cast Ph_2TDPP film is also reported, showing typical features of *J*-aggregates formation.[42]

A spin-cast *c*-EXG-TDPP thin film on an ITO conductive substrate was studied through scanning electron microscopy (SEM) and the corresponding top-view images are reported in Figure 4a and 4b. At this resolution, it is possible to recognize the presence of homogeneously distributed graphene flakes with sizes ranging from 500 nm to 1 µm (the nanostructured background is due to the high-roughness of the ITO surface). The size of the graphene agglomerates present in the *c*-EXG-TDPP film is confirmed by dynamic light scattering analysis in solution (Figure S3 in the S.I.). More in detail, Figure 4b shows a zoom on a graphene flake in both secondary and back-scattered electrons mode, this last one allowing to better evidence the contrast between different atomic weights, with the darker carbon-based component emerging more clearly from the ITO background. These images

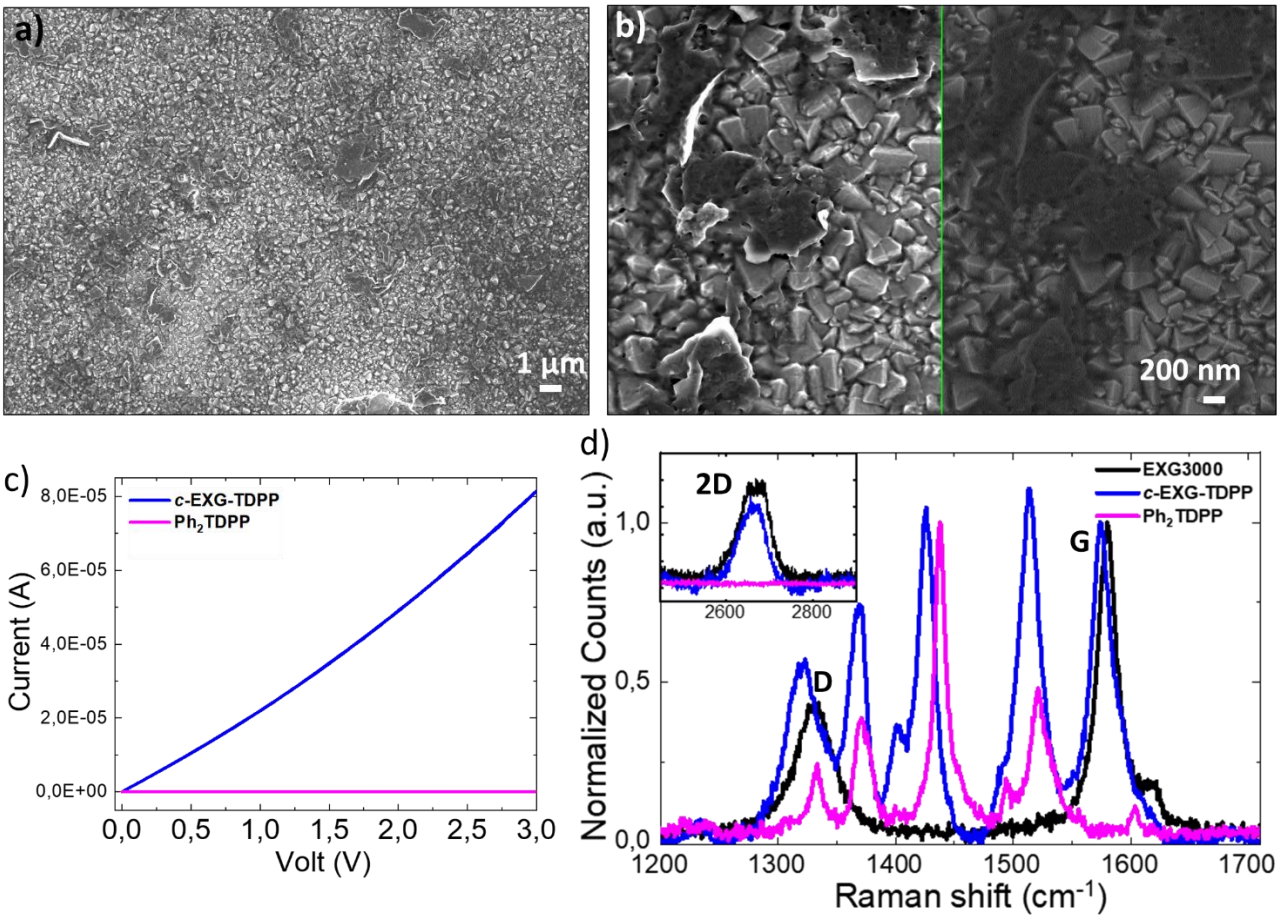

Figure 4. a) Scanning electron microscopy top-view image of a spin-coated thin film of the cross-linked graphene-diketopyrrolopyrrole hybrid (*c*-EXG-TDPP) on a conductive glass slide (indium tin oxide – ITO). The background crystalline nanostructures are due to the ITO intrinsic roughness. b) Comparison between the secondary electron image (left) and the back-scattered electron image (right) of the same sample as in a) at higher magnification. c) Electrical conductivity of *c*-EXG-TDPP and of reference Ph_2TDPP spin-coated thin films. d) Comparison of Raman spectrum of *c*-EXG-TDPP with that of the reference Ph_2TDPP dye and of the pristine graphene (EXG 3000). The inset shows the 2D band area of the spectra.

are very useful to describe the *c*-EXG-TDPP nature as that of a polymer nanocomposite, containing TDPP oligomeric units that connect well-dispersed graphene flakes. The TDPP oligomerization likely proceeds through biaryl coupling reactions that compete with the aryl radical addition to the graphene surface.[43] Such a competing reaction has a higher probability of happening in a bi-functional aniline system, such as that used for the production of *c*-EXG-TDPP than in a mono-aniline one, as for EXG-TDPP, where, in addition, the coupling should proceed between an aryl radical and a pendant thiophene. The SEM images also allow stating that the *in-situ* Tour reaction has led to the partial disruption of the pristine EXG 3000 flakes.

The presence of a graphene component provides electrical conductivity to spin-cast thin films of *c*-EXG-TDPP, as can be seen from Figure 4c, differently from the case of films of the sole reference

OSC Ph_2TDPP (an electrical resistance of around 40 KΩ is found in the graphene-TDPP nanocomposite film).

Raman analysis is further useful to support the covalent functionalization of graphene that provides *c*-EXG-TDPP as the final product. Figure 4d reports a comparison of Raman spectra of *c*-EXG-TDPP, the graphene precursor EXG 3000 and the reference small molecule Ph_2TDPP in the region of the D and G bands. These two bands are marked with labels in the figure and the D-to-G band intensity ratio (I_D/I_G) is estimated from the spectra to change from 0.44 in EXG-3000 to 0.55 in *c*-EXG-TDPP. This indicates the generation of an increased number of sp^3defects in the graphene scaffold, following functionalization (a control experiment in which EXG 3000 was treated with isopentyl nitrite in the same conditions but in the absence of the di-aniline derivative showed no changes in I_D/I_G, stating the generation of covalent functionalization derived sp^3 defects in the graphene scaffolds). An I_D/I_G of 0.44 for EXG 3000 (starting from a 0.2 value in Madagascar graphite, not shown) is in agreement with previous reports and the nature of defects in the material should be mainly attributed to edges in the sheets, even if the formation of some topological defects in the basal plane cannot be excluded.[36,44] The intensity of the 2D band (inset in Figure 3) decreases after functionalization, also in agreement with the introduction of sp^3 defects in the basal plane. Interestingly, from the comparison of Raman spectra of *c*-EXG-TDPP and Ph_2TDPP, significant variations in the chromophore peaks are observed after covalent grafting, both in position and intensity, reasonably consistent with the establishment of an electronic coupling between the OSC part and the graphene part of the composite. The parameter I_D/I_G cannot be employed for estimating the functionalization degree (FD) of graphene: the analysis of the Raman spectrum of EXG-TDPP (Figure S4 in the S.I.) shows a different I_D/I_G for this species (2.59), which seems to indicate a significantly higher FD, even if the reactants were employed in the same stoichiometric amounts (only a factor 2 could be considered as difference in reactive sites on the two TDPP anilines, which does not count for such a higher I_D/I_G). Unfortunately also TGA, which can be employed in some cases for determining FD (as we also did in the past, see refs. [6,7,9,10]), is in the present case not useful, since the degradation of EXG 3000 starts already when the covalently linked organic moieties are degrading, thus causing an overlapping of the thermal decomposition trends. Some information on the identity of the samples can be derived from TGA traces collected under nitrogen, reported in Figure S5 in the S.I.: from these curves it appears indeed that the quantity of graphene in the cross-linked species *c*-EXG-TDPP is higher than in EXG-TDPP, as the un-burned residue at 1000 °C is significantly higher for the former (and almost 30% lower than for pristine EXG 3000) compared to the latter. This would somehow point out at a large dye/graphene ratio in EXG-TDPP compared to *c*-EXG-TDPP, as Raman seems to indicate.

The photophysics of *c*-EXG-TDPP was studied to understand the nature of the interactions between the oligomeric OSC component and graphene. PL properties were first investigated for the composite system and compared to those of the reference small molecule Ph_2TDPP. The SS-PL spectra of the two species in DMF solution at the same concentration are reported in Figure 5a. Ph_2TDPP is characterized by a strong emission at 612 nm featuring a vibronic progression with bands at 659, 740 and 825 nm, while the fluorescence from the *c*-EXG-TDPP solution is almost completely quenched. The main reason for this phenomenon is related to well-known graphene PL quenching properties, generally driven by a Förster Resonance Energy Transfer (FRET) process, that takes place between the chromophore and the GBM scaffold.[45]

Given the complex nature of the composite samples, TR-PL analysis can be particularly useful to unveil additional details of their photophysics. Indeed, fluorescence lifetime is strongly influenced by the chemical composition of the emitter's environment and by the presence of additional processes like FRET, quenching, charge transfer, solvation dynamics, etc. Changes in the fluorescence decay dynamics can therefore be used to gain information about the local chemical environment.

In Figure 5b the TR-PL decays are plotted. The reference small molecule Ph_2TDPP is characterized by a simple mono-exponential fluorescence decay from which a lifetime of 3.8 ns can be deduced, in agreement with what already found for similar molecules.[46] For the *c*-EXG-TDPP sample, the fluorescence decay has instead a more complex bi-exponential behavior characterized by two distinct time constants (τ_1 = 1.7 ns and τ_2 = 3.8 ns). Considering the Ph_2TDPP decay, we can assign these two lifetimes to two different emissive species present in the composite, namely the dye units directly bound to graphene, with the fastest emissive lifetime, and the oligomeric TDPP unit not directly connected to graphene, with the slowest one. In order to gain more information on the surface coverage distribution of these TDPP oligomers within the films, we performed FLIM analysis, which can be easily correlated to SEM top view images. In Figure 5c and 5d the FLIM images of *c*-EXG-TDPP and Ph_2TDPP thin films on glass slides are reported. Average lifetimes are now reduced with respect to solutions, as it usually happens at the solid state.[47] In the graphene-containing film the intensity-weighted average lifetime is lower with respect to the dye film, inferring the influence of graphene PL quenching effects. Moreover, by observing Figure 5c in detail, several areas emerge on the surface in which the lifetime is further reduced to approximately 0.1 ns, close to the instrument resolution. After proper comparison with SEM images, we can hypothesize that these areas are constituted of graphene flakes, locally strongly quenching the PL of those TDPP molecules that are directly bound to them. On the other hand, from this image it is possible to highlight that the presence of graphene flakes does not contribute to generate pinholes in the film (at least at a microscale resolution) and that the film is indeed highly homogeneous.

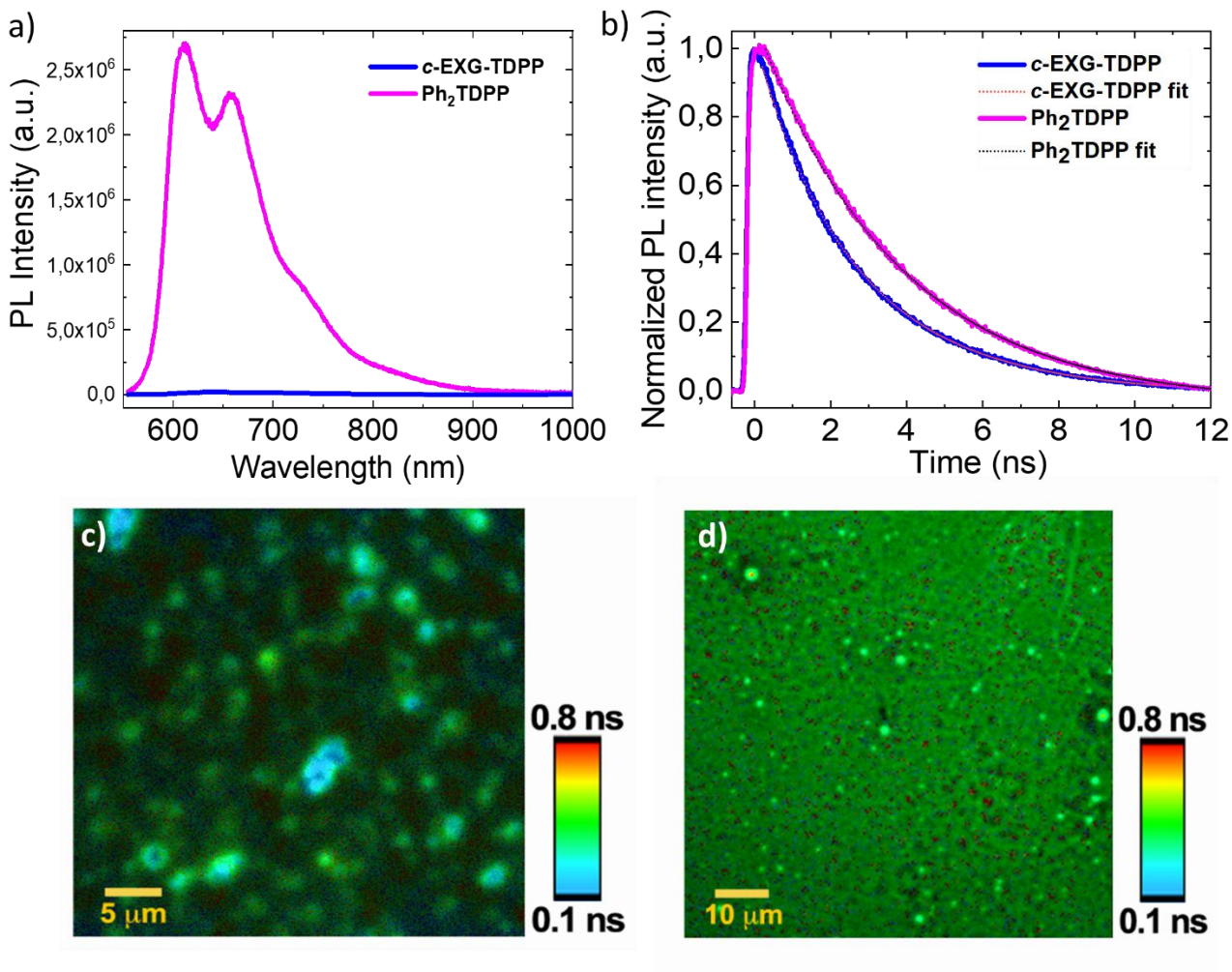

Figure 5. Characterization of the emissive properties of the cross-linked graphene-diketopyrrolopyrrole hybrid (*c*-EXG-TDPP). a) Comparison of the steady-state photoluminescence spectra of iso-absorbing solutions of *c*-EXG-TDPP and its reference dye (Ph_2TDPP) in DMF solution (λ_{exc} = 530 nm) b) Time-resolved photoluminescence decays of c-EXG-TDPP and Ph_2TDPP in DMF solution under excitation at 400 nm. The 2-exponential fits of the two decays are also reported. For *c*-EXG-TDPP two lifetimes are found, namely τ_1 = 1.7 ns (A_1 = 52%) and τ_2 = 3.8 ns (A_2 = 48%). For the free dye Ph_2TDPP, only one lifetime is detected, τ_1 = 3.8 ns. c,d) Intensity-weighted fluorescence lifetime maps of, respectively, a *c*-EXG-TDPP and a Ph_2TDPP spin-coated films on glass slides.

To investigate more thoroughly the photophysics and photochemistry of the graphene-TDPP composite we resorted to EPR spectroscopy, a technique that has been successfully employed for the detection of several photo-generated intermediate species in photoactive materials.[48] In particular, by means of EPR spectroscopy it is often possible to detect the generation and decay of charge separated states, which in organic materials are usually unpaired electron species, *i.e.* radicals, after visible photoexcitation of a material.[10,49] The identification of the photogenerated radical is an important piece of information for the thorough description of the photoinduced processes taking place in the material.

For this purpose, we recorded several EPR spectra of *c*-EXG-TDPP and of the Ph_2TDPP reference small molecule under continuous white light illumination (Figure 6a). The *c*-EXG-TDPP as prepared (d0 of the illumination) shows a rather strong EPR peak, as it is well seen in Figure 6a (left panel, black curve). A similar but weaker spectrum is obtained from the pristine EXG 3000 graphene sample (Figure 6a, left panel, orange dashed curve). As a control experiment, we also recorded the EPR spectrum of the reference dye, which does not show any EPR feature at d0 (Figure 6a, right panel, dark curve). In detail, the EPR spectra of both the graphene-dye hybrid and pristine graphene are composed of a broad unsymmetrical line at about 100 Gauss centered at a magnetic field corresponding to a g-factor of 2.0045, with a narrower feature centered at $g = 2.0027 \pm 0.0005$. The narrow peak is more intense in the composite sample, indicating that the paramagnetic species responsible for this peak increases after the functionalization of graphene. We assign this EPR signal to defect sites in graphitic-type carbon. A large variety of defect sites revealed with EPR have been reported in literature but there are still many uncertainties on the assignments.[50,51] It is interesting to note that the functionalization of EXG 3000 causes the increase of only a subset of the defects, which are probably related to isolated and confined aromatic regions where an unpaired electron is trapped.[52] Because of the almost negligible change in line intensity with respect to samples in dark before the illumination test (not shown here for the sake of clarity), we further assume that the signal is originated from parts of the composite material where the local environment allows the formation of radicals due to inhomogeneity and it could be correlated to the inhomogeneous lifetimes found in the FLIM image in Figure 5c.The bulk material is likely not producing a substantial number of radicals, as it would be expected if an effective charge separation in the composite was taking place. In view of the above results, we suggest that the fate of the excess energy accumulated in the material after light absorption is dominated by dissipation through energy transfer and thermal deactivation, without a consistent production of free radicals or other paramagnetic species. Therefore, the quenching of the TDPP PL in *c*-EXG-TDPP can be undoubtedly attributed to a fast energy transfer/thermalization and not to a charge transfer processes. To complete the scenario, we further investigated the eventual presence of PL signals in the far-red to NIR range in *c*-EXG-TDPP but no signal was detected, as reported in Figure S6 in the S.I.

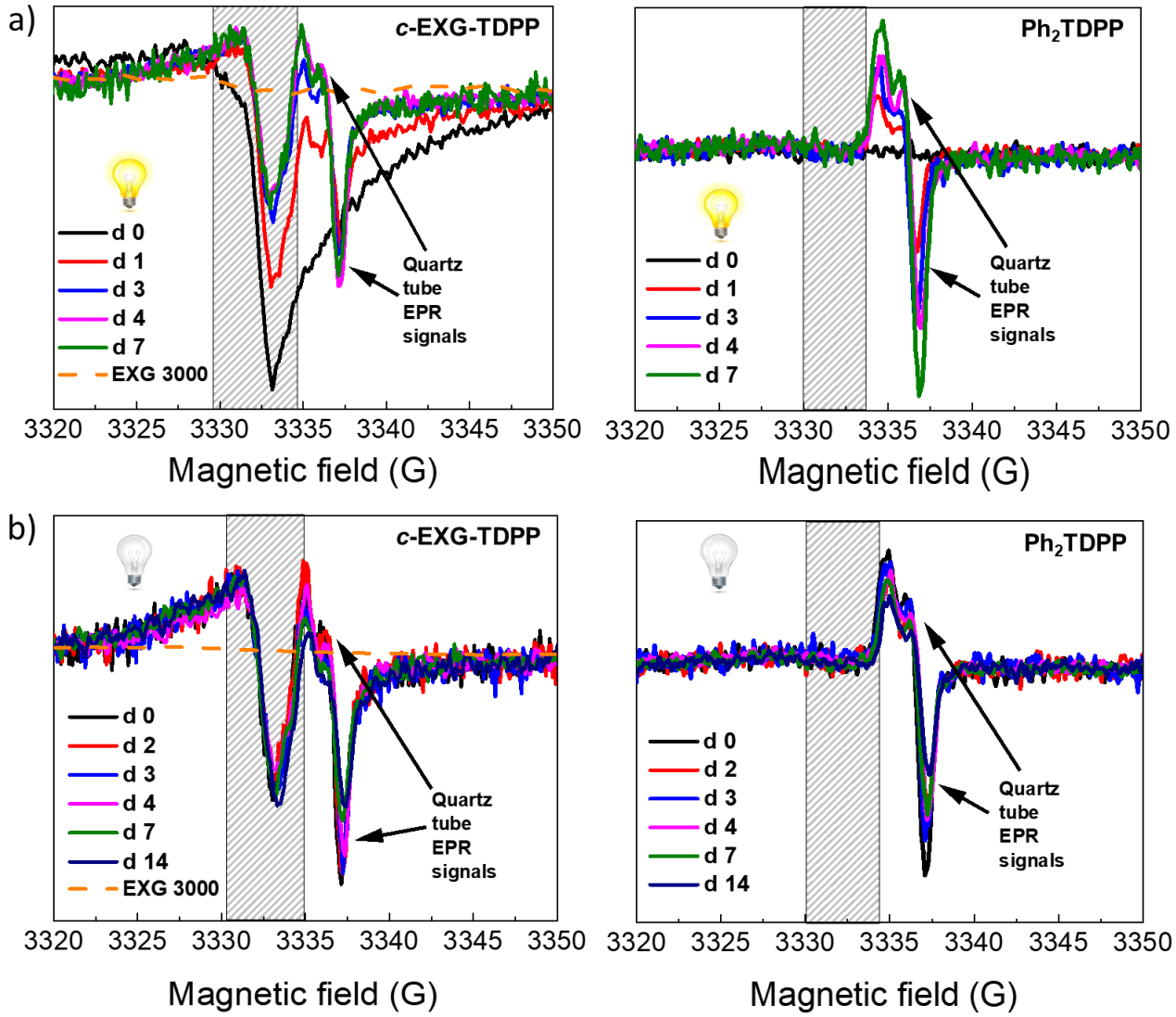

Figure 6. Electron paramagnetic resonance characterization of the cross-linked graphene-diketopyrrolopyrrole hybrid (*c*-EXG-TDPP) compared to the reference Ph_2TDPP dye and pristine graphene (EXG 3000). a) Light-induced spectra obtained during 7 days illumination of *c*-EXG-TDPP (left) and Ph_2TDPP (right) degassed solutions in toluene with a Xe lamp (150 W). The arrows indicate the signal of the quartz tubes in which the measurements are conducted. b) Spectra of the same samples as in a) after irradiation, kept in the dark for 14 days. The signal of EXG 3000 (orange dashed line) did not show any variation during illumination and recovery in dark and therefore is reported as a single spectrum in a) and b) for the sake of clarity.

In order to probe the photo-stability of *c*-EXG-TDPP, we realized an endurance test in which the samples (*c*-EXG-TDPP and Ph_2TDPP) were continuously illuminated for one week at high power (~50 mW cm^{-2}) and then subjected to a subsequent recovery period in dark, while measuring EPR spectra each day (Figure 6a and 6b). Figure 6a interestingly shows that during the light soaking process, the EPR signal is partially reduced in *c*-EXG-TDPP, until it reaches a plateau after one week. On the other hand, the reference dye sample does not show any signal variation. This phenomenon detected in the composite can be explained considering a passivation of the un-paired radical defects

through the interaction with the solvent medium (in this case toluene) mediated by π-interactions. The fact that the free dye does not show any signal variation is easily explained by the fact that a single molecule, when irradiated, quickly passivates photo-generated spins with a shorter time constant than the measurement itself: this evidence further corroborates the idea of a polymer-like structure for the *c*-EXG-TDPP sample. The recovery test performed for 14 days after the irradiation is shown in Figure 6b. Both the samples remain stable in this timeframe, therefore we can argue that the modification occurred during the light soaking test is almost irreversible.

4. Conclusions

In this work we reported the synthesis and characterization of a covalent hybrid species obtained by good quality graphene flakes prepared through mechanical exfoliation of commercially available graphite and a diketopyrrolopyrrole-based OSC. A detailed investigation of this material allows us to state its nature of cross-linked polymer composite, with a disordered structure based on TDPP oligomeric units bridging homogeneously distributed graphene flakes. In this regard, we can predict that phase separation in such a composite, given the presence of covalent bonds, is unlikely to happen. The composite is highly soluble in organic solvents and can be cast into thin films, characterized by a blue color and semi-transparent. In this regard, it is also particularly attractive the electrical conductivity that these films shows, which make them interesting candidates for applications as anti-static coatings.

The photophysical insights gained on such a graphene-OSC polymer nanocomposite, that we derived from emission spectroscopy and EPR analysis, points out at a very effective quenching of the absorbed photon energy through mechanisms not involving charge transfer or other radical-forming processes. Indeed, this is strong evidence of an effective photo-protecting action that this material could exert, as a consequence of its intrinsic photo-stability.

We argue therefore that our graphene-diketopyrroloryrrole cross-linked covalent hybrid might open new perspectives for the development of film-forming materials with potentially broad applications in the field of thin film photo-protective layers with good electrical properties and with the additional peculiarity of tunable colors, achievable by changing the OSC component, coupled to semi-transparency.

Acknowledgments

M.Z. thanks Fondazione Cariparo for a PhD scholarship. E.C. and I.F. acknowledge financial support from the MIUR through PRIN 2015 no. 2015XBZ5YA and ‘NExuS’ - Department of Excellence Program. A.K. thanks financial support from the Hungarian National Research, Development and

Innovation Office through the K 126065 and 2018-2.1.12-TÉT-HR-2018-00009 projects is acknowledged. A.M. acknowledges funding by EPSRC (grant EP/P006280/1, MARVEL). F.C. is a Royal Society Wolfson Foundation Merit Award holder. T.G. acknowledges DFG financial support via the GRK (Research Training Group) 2204 "Substitute Materials for sustainable Energy Technologies" and Prof. Igor Djerdj for insightful advice.

References

[1] C.-H. Kim, I. Kymissis, Graphene–organic hybrid electronics, J. Mater. Chem. C. 5 (2017) 4598–4613.

[2] Y. Zhao, S. Ippolito, P. Samorì, Functionalization of 2D Materials with Photosensitive Molecules: From Light-Responsive Hybrid Systems to Multifunctional Devices, Adv. Opt. Mater. (2019) 1900286.

[3] X. Zhang, L. Hou, P. Samorì, Coupling carbon nanomaterials with photochromic molecules for the generation of optically responsive materials, Nat. Commun. 7 (2016) 11118.

[4] M. Gobbi, S. Bonacchi, J.X. Lian, A. Vercouter, S. Bertolazzi, B. Zyska, M. Timpel, R. Tatti, Y. Olivier, S. Hecht, M. V Nardi, D. Beljonne, E. Orgiu, P. Samorì, Collective molecular switching in hybrid superlattices for light-modulated two-dimensional electronics, Nat. Commun. 9 (2018) 2661.

[5] F. Bonaccorso, N. Balis, M.M. Stylianakis, M. Savarese, C. Adamo, M. Gemmi, V. Pellegrini, E. Stratakis, E. Kymakis, Functionalized Graphene as an Electron-Cascade Acceptor for Air-Processed Organic Ternary Solar Cells, Adv. Funct. Mater. 25 (2015) 3870–3880.

[6] T. Gatti, F. Lamberti, P. Topolovsek, M. Abdu-Aguye, R. Sorrentino, L. Perino, M. Salerno, L. Girardi, C. Marega, G.A. Rizzi, M.A. Loi, A. Petrozza, E. Menna, Interfacial Morphology Addresses Performance of Perovskite Solar Cells Based on Composite Hole Transporting Materials of Functionalized Reduced Graphene Oxide and P3HT, Sol. RRL. 2 (2018) 1800013.

[7] T. Gatti, S. Casaluci, M. Prato, M. Salerno, F. Di Stasio, A. Ansaldo, E. Menna, A. Di Carlo, F. Bonaccorso, Boosting Perovskite Solar Cells Performance and Stability through Doping a Poly-3(hexylthiophene) Hole Transporting Material with Organic Functionalized Carbon Nanostructures, Adv. Funct. Mater. 26 (2016) 7443-7453.

[8] C.J. Shearer, A. Cherevan, D. Eder, Application and Future Challenges of Functional Nanocarbon Hybrids, Adv. Mater. 26 (2014) 2295–2318.

[9] T. Gatti, N. Manfredi, C. Boldrini, F. Lamberti, A. Abbotto, E. Menna, A D-π-A organic dye – Reduced graphene oxide covalent dyad as a new concept photosensitizer for light harvesting applications, Carbon 115 (2017) 746-753.

[10] P. Guarracino, T. Gatti, N. Canever, M. Abdu-Aguye, M.A. Loi, E. Menna, L. Franco, Probing photoinduced electron-transfer in graphene-dye hybrid materials for DSSC, Phys. Chem. Chem. Phys. 19 (2017) 27716–27724.

[11] G. Bottari, M.Á. Herranz, L. Wibmer, M. Volland, L. Rodríguez-Pérez, D.M. Guldi, A. Hirsch, N. Martín, F. D'Souza, T. Torres, Chemical functionalization and characterization of graphene-based materials, Chem. Soc. Rev. 46 (2017) 4464–4500.

[12] L. Rodríguez-Pérez, M. a Á. Herranz, N. Martín, The chemistry of pristine graphene, Chem. Commun. 49 (2013) 3721–3735.

[13] V. Georgakilas, M. Otyepka, A.B. Bourlinos, V. Chandra, N. Kim, K.C. Kemp, P. Hobza, R. Zboril, K.S. Kim, Functionalization of Graphene: Covalent and Non-Covalent Approaches, Derivatives and Applications, Chem. Rev. 112 (2012) 6156–6214.

[14] G.L.C. Paulus, Q.H. Wang, M.S. Strano, Covalent Electron Transfer Chemistry of Graphene with Diazonium Salts, Acc. Chem. Res. 46 (2013) 160–170.

[15] J.L. Bahr, J.M. Tour, Highly Functionalized Carbon Nanotubes Using in Situ Generated

Diazonium Compounds, Chem. Mater. 13 (2001) 3823–3824.
[16] F. Lamberti, S. Salmaso, A. Zambon, L. Brigo, A. Malfanti, T. Gatti, S. Agnoli, G. Granozzi, G. Brusatin, N. Elvassore, M. Giomo, A Combined Electrochemical-Microfluidic Strategy for the Microscale-Sized Selective Modification of Transparent Conductive Oxides, 5 (2018) 1701222.
[17] S. Silvestrini, C.C. De Filippo, N. Vicentini, E. Menna, R. Mazzaro, V. Morandi, L. Ravotto, P. Ceroni, M. Maggini, Controlled Functionalization of Reduced Graphene Oxide Enabled by Microfluidic Reactors, Chem. Mater. 30 (2018) 2905–2914.
[18] K. Zhao, T. Zhang, H. Chang, Y. Yang, P. Xiao, H. Zhang, C. Li, C.S. Tiwary, P.M. Ajayan, Y. Chen, Super-elasticity of three-dimensionally cross-linked graphene materials all the way to deep cryogenic temperatures, Sci. Adv. 5 (2019) 2589.
[19] W. Chen, P. Xiao, H. Chen, H. Zhang, Q. Zhang, Y. Chen, Polymeric Graphene Bulk Materials with a 3D Cross-Linked Monolithic Graphene Network, Adv. Mater. 31 (2019) 1802403.
[20] S. Qu, H. Tian, Diketopyrrolopyrrole (DPP)-based materials for organic photovoltaics, Chem. Commun. 48 (2012) 3039–3051.
[21] W. Li, K.H. Hendriks, M.M. Wienk, R.A.J. Janssen, Diketopyrrolopyrrole Polymers for Organic Solar Cells, Acc. Chem. Res. 49 (2016) 78–85.
[22] A. Tang, C. Zhan, J. Yao, E. Zhou, Design of Diketopyrrolopyrrole (DPP)-Based Small Molecules for Organic-Solar-Cell Applications, Adv. Mater. 29 (2017) 1600013.
[23] Y. Li, P. Sonar, L. Murphy, W. Hong, High mobility diketopyrrolopyrrole (DPP)-based organic semiconductor materials for organic thin film transistors and photovoltaics, Energy Environ. Sci. 6 (2013) 1684–1710.
[24] O. Fenwick, S. Fusco, T.N. Baig, F. Di Stasio, T.T. Steckler, P. Henriksson, C. Fléchon, M.R. Andersson, F. Cacialli, Efficient red electroluminescence from diketopyrrolopyrrole copolymerised with a polyfluorene, APL Mater. 1 (2013) 32108.
[25] M. Sassi, N. Buccheri, M. Rooney, C. Botta, F. Bruni, U. Giovanella, S. Brovelli, L. Beverina, Near-infrared roll-off-free electroluminescence from highly stable diketopyrrolopyrrole light emitting diodes, Sci. Rep. 6 (2016) 34096.
[26] M. Kaur, D.H. Choi, Diketopyrrolopyrrole: brilliant red pigment dye-based fluorescent probes and their applications, Chem. Soc. Rev. 44 (2015) 58–77.
[27] O. Wallquist, R. Lenz, 20 years of DPP pigments – future perspectives, Macromol. Symp. 187 (2002) 617–630.
[28] J. Dhar, D.P. Karothu, S. Patil, Herringbone to cofacial solid state packing via H-bonding in diketopyrrolopyrrole (DPP) based molecular crystals: influence on charge transport, Chem. Commun. 51 (2015) 97–100.
[29] B. Soberats, M. Hecht, F. Würthner, Diketopyrrolopyrrole Columnar Liquid-Crystalline Assembly Directed by Quadruple Hydrogen Bonds, Angew. Chemie Int. Ed. 56 (2017) 10771–10774.
[30] J. Ma, Z. Liu, Z. Wang, Y. Yang, G. Zhang, X. Zhang, D. Zhang, Charge mobility enhancement for diketopyrrolopyrrole-based conjugated polymers by partial replacement of branching alkyl chains with linear ones, Mater. Chem. Front. 1 (2017) 2547–2553.
[31] S.-F. Yang, X. Zhang, P.-L. Chen, Z.-T. Liu, J.-W. Tian, G.-X. Zhang, D.-Q. Zhang, Diketopyrrolopyrrole-Based Semiconducting Polymer with Both Hydrophobic Alkyl and Hydrophilic Tetraethylene Glycol Chains for Monolayer Transistor and Sensing Application, Adv. Electron. Mater. 3 (2017) 1700120.
[32] R. Yadav, M. Tirumali, X. Wang, M. Naebe, B. Kandasubramanian, Polymer composite for antistatic application in aerospace, Def. Technol. (2019). doi:https://doi.org/10.1016/j.dt.2019.04.008.
[33] Y. Wang, K. Huang, A. Derré, P. Puech, S. Rouzière, P. Launois, C. Castro, M. Monthioux, A. Pénicaud, Conductive graphene coatings synthesized from graphenide solutions, Carbon 121 (2017) 217–225.

[34] C. Luo, L. Zhou, K. Chiou, J. Huang, Multifunctional Graphene Hair Dye, Chem. 4 (2018) 784–794.
[35] F. Jonas, W. Krafft, B. Muys, Poly(3, 4-ethylenedioxythiophene): Conductive coatings, technical applications and properties, Macromol. Symp. 100 (1995) 169–173.
[36] K.R. Paton, E. Varrla, C. Backes, R.J. Smith, U. Khan, A. O'Neill, C. Boland, M. Lotya, O.M. Istrate, P. King, T. Higgins, S. Barwich, P. May, P. Puczkarski, I. Ahmed, M. Moebius, H. Pettersson, E. Long, J. Coelho, S.E. O'Brien, E.K. McGuire, B.M. Sanchez, G.S. Duesberg, N. McEvoy, T.J. Pennycook, C. Downing, A. Crossley, V. Nicolosi, J.N. Coleman, Scalable production of large quantities of defect-free few-layer graphene by shear exfoliation in liquids, Nat. Mater. 13 (2014) 624.
[37] M.I. Kairi, S. Dayou, N.I. Kairi, S.A. Bakar, B. Vigolo, A.R. Mohamed, Toward high production of graphene flakes – a review on recent developments in their synthesis methods and scalability, J. Mater. Chem. A. 6 (2018) 15010–15026.
[38] V. Singh, D. Joung, L. Zhai, S. Das, S.I. Khondaker, S. Seal, Graphene based materials: Past, present and future, Prog. Mater. Sci. 56 (2011) 1178–1271.
[39] A.C. Ferrari, J.C. Meyer, V. Scardaci, C. Casiraghi, M. Lazzeri, F. Mauri, S. Piscanec, D. Jiang, K.S. Novoselov, S. Roth, A.K. Geim, Raman Spectrum of Graphene and Graphene Layers, Phys. Rev. Lett. 97 (2006) 187401.
[40] X. Zeng, Z. Li, J. Ren, T. Ge, Z. Zang, Q. Sun, H. Wang, Y. Hao, Low bandgap diketopyrrolopyrrole-based polymers with an asymmetric unit of fluoridated phenylene-thiophene for efficient polymer solar cells, Synth. Met. 240 (2018) 30–36.
[41] K.H. Hendriks, W. Li, G.H.L. Heintges, G.W.P. van Pruissen, M.M. Wienk, R.A.J. Janssen, Homocoupling Defects in Diketopyrrolopyrrole-Based Copolymers and Their Effect on Photovoltaic Performance, J. Am. Chem. Soc. 136 (2014) 11128–11133.
[42] R. Heuvel, F.J.M. Colberts, J. Li, M.M. Wienk, R.A.J. Janssen, The effect of side-chain substitution on the aggregation and photovoltaic performance of diketopyrrolopyrrole-alt-dicarboxylic ester bithiophene polymers, J. Mater. Chem. A. 6 (2018) 20904–20915.
[43] P. Salice, E. Fabris, C. Sartorio, D. Fenaroli, V. Figà, M.P. Casaletto, S. Cataldo, B. Pignataro, E. Menna, An insight into the functionalisation of carbon nanotubes by diazonium chemistry: Towards a controlled decoration, Carbon 74 (2014) 73–82.
[44] U. Khan, A. O'Neill, M. Lotya, S. De, J.N. Coleman, High-Concentration Solvent Exfoliation of Graphene, Small. 6 (2010) 864–871.
[45] F. Lamberti, L. Brigo, M. Favaro, C. Luni, A. Zoso, M. Cattelan, S. Agnoli, G. Brusatin, G. Granozzi, M. Giomo, N. Elvassore, Optoelectrochemical Biorecognition by Optically Transparent Highly Conductive Graphene-Modified Fluorine-Doped Tin Oxide Substrates, ACS Appl. Mater. Interfaces. 6 (2014) 22769–22777.
[46] S. Türkçen, H. Dinçalp, G. murat saltan, Synthesis and determination of fluorescence properties of new soluble diketopyrrolopyrrole type photosensitizers, J. Mol. Struct. 1195 (2019) 485–493.
[47] J.R. Lakowicz, Principles of fluorescence spectroscopy, Second edition. New York : Kluwer Academic/Plenum, (1999)
[48] J. Niklas, O.G. Poluektov, Organic Photovoltaics: Charge Transfer Processes in OPV Materials as Revealed by EPR Spectroscopy, Adv. Energy Mater. 7 (2017) 1602226.
[49] F. Lamberti, T. Gatti, E. Cescon, R. Sorrentino, A. Rizzo, E. Menna, G. Meneghesso, M. Meneghetti, A. Petrozza, L. Franco, Evidence of Spiro-OMeTAD De-doping by tert-Butylpyridine Additive in Hole-Transporting Layers for Perovskite Solar Cells, Chem. 5 (2019) 1806-1817.
[50] A. Barbon, EPR spectroscopy in the study of 2D graphene-based nanomaterials and nanographites, in: Electron Paramagn. Reson. Vol. 26, The Royal Society of Chemistry, (2019) 38–65.
[51] F. Tampieri, S. Silvestrini, R. Riccò, M. Maggini, A. Barbon, A comparative electron

paramagnetic resonance study of expanded graphites and graphene, J. Mater. Chem. C. 2 (2014) 8105–8112.
[52] J. Hong, E. Bekyarova, W.A. de Heer, R.C. Haddon, S. Khizroev, Chemically Engineered Graphene-Based 2D Organic Molecular Magnet, ACS Nano. 7 (2013) 10011–10022.